Contemporary Mathematics
https://ojs.wiserpub.com/index.php/CM/

Research Article

Thermodynamic Features of a Heat Engine with an Exponentially Decreasing Temperature Profile

Mesfin Asfaw Taye

West Los Angeles College, Science Division, 9000 Overland Ave, Culver City, CA, 90230, USA
E-mail: tayem@wlac.edu

Received: 16 April 2025; **Revised:** 12 May 2025; **Accepted:** 19 May 2025

Abstract: In this study, we advance the understanding of nonequilibrium systems by deriving thermodynamic relations for a heat engine operating under an exponentially decreasing temperature profile. Such thermal configurations closely mimic spatially localized heating, such as laser-induced thermal gradients. Using exact analytical solutions, we show that this arrangement results in significantly higher velocity, entropy production, and extraction rates than piecewise thermal profiles, while exhibiting reduced irreversibility and complexity relative to linear or quadratic gradients. We further examine the thermodynamic behavior of the Brownian particles in the networks. Our study reveals that the velocity and entropy production rates remain independent of the network size; in contrast, extensive quantities, such as total entropy, depend on the number of microstates. Additionally, we show that a Brownian particle in a ratchet potential with spatially varying temperature achieves directed motion, even without external forces driven solely by thermal asymmetry. These findings highlight the critical role of temperature asymmetry in controlling transport processes and optimizing particle dynamics. This will have promising applications in microfluidic devices and nanoscale sensors. Finally, we explore the influence of the system parameters on the efficiency and performance of the heat engine. The exponential temperature profiles enable faster velocities while simultaneously exhibiting higher efficiency compared to other thermal arrangements. Moreover, by addressing key questions on entropy production, we provide insights into the transition between nonequilibrium and equilibrium systems and contribute tools for optimizing energy-efficient systems in both natural and engineered settings.

***Keywords*:** Brownian motor, nonequilibrium thermodynamics, entropy production, heat engine, temperature gradient

MSC: 82C05

1. Introduction

Nonequilibrium thermodynamics and statistical mechanics remain challenging because of the complexity of systems that are far from equilibrium. Unlike equilibrium systems, which follow well-defined principles such as the Boltzmann distribution, nonequilibrium systems lack a universal framework. Key challenges include understanding microscopic entropy production, predicting steady-state distributions, and addressing the impact of rare fluctuations. Although advances such as the thermodynamic uncertainty relation offer insights, a complete understanding of nonequilibrium processes remains incomplete, highlighting the need for better theoretical and experimental approaches.

DOI: https://doi.org/10.37256/cm.6420257028

Recent studies on nonequilibrium thermodynamic systems have garnered significant attention owing to their profound implications in science and technology [1–22]. Research efforts have explored both classical [18, 19] and quantum systems [20–22] with a particular focus on entropy production. The dependence of entropy production was investigated using the master equation approach for discrete systems [1–5] and the Fokker-Planck equation for continuous systems [7, 8, 13, 23, 24]. Various thermodynamic relations have been derived using stochastic thermodynamics [6], time-reversal operations [25, 26], and the fluctuation theorem [27–29]. The Thermodynamic Uncertainty Relation (TUR) has recently emerged as a fundamental framework for estimating entropy production from time-series data [30–34]. Recent studies have extended entropy production analysis to non-Markovian systems [35].

In our previous studies, we investigated the thermodynamic properties of Brownian heat engines operating in heat baths with temperature profiles that decrease quadratically [36], linearly, or in a piecewise constant manner [37]. Using the Boltzmann-Gibbs nonequilibrium entropy framework and entropy balance equation, we analyzed key thermodynamic quantities such as entropy production and extraction rates by solving the system dynamics over time. Our findings highlight that the quadratic temperature profile yields the lowest efficiency but the highest particle velocity compared with the other arrangements. Understanding these thermodynamic relationships is crucial for predicting energy dissipation and optimizing transport efficiency in biological systems.

This study advances the understanding of nonequilibrium systems by deriving thermodynamic relations for a heat engine operating under an exponentially decreasing temperature profile. This arrangement offers valuable insights into entropy production, energy dissipation, and transport dynamics. Such an arrangement is particularly relevant because it mimics the temperature distribution in local heating scenarios, such as systems heated by a laser beam, where the heat decreases spatially. Our exact analytical solution reveal that the velocity, entropy production, and extraction rates were significantly higher than those in piecewise thermal arrangements. In addition, we describe the thermodynamic behavior of Brownian particles moving through networks. The results show that thermodynamic quantities, such as velocity and entropy production rate, are independent of network size, whereas extensive quantities, such as total entropy, depend on the number of microstates. Systems with exponentially decreasing temperature gradients exhibit much lower entropy production and extraction rates than those with linearly or quadratically varying profiles, indicating reduced irreversibility and complexity introduced by such thermal baths. In this work, we study a Brownian heat engine operating in a ratchet potential coupled to a spatially varying temperature field with exponential decay. Such configurations are not only analytically tractable but also experimentally relevant, as they mimic systems with localized heating-such as laser-induced temperature gradients observed in microfluidic and nanoscale environments. The goal is to derive exact thermodynamic quantities, including entropy production, extraction rates, and velocity, and to explore their behavior under nonequilibrium conditions.

We also show that a Brownian particle in a ratchet potential with spatially varying temperature achieves directed motion, even in the absence of external forces. The thermal asymmetry and applied load generate a net particle current, offering insights into microscale and nanoscale transport systems in which controlled motion is crucial. Notably, adjusting the thermal arrangement alone enabled directed motion. Moreover, by tuning the system parameters, such as barrier height, load, and noise intensity, the particle velocity can be optimized. This, in turn, helps improve the efficiency of microfluidic devices and nanoscale sensors. We believe that these findings will deepen our understanding of thermally driven ratchets and the critical role of temperature asymmetry in Brownian motors. Moreover, we explore how the efficiency and Coefficient of Performance (*COP*) depend on the motor parameters. Although these motors are generally less efficient than those operating in piecewise thermal arrangements, they achieve higher velocities. Conversely, they exhibit higher efficiencies but lower velocities than motors that function in linearly or quadratically decreasing thermal environments. Thus, this study enhances the understanding of thermally driven ratchets, highlighting the role of temperature asymmetry in controlling transport processes across various physical systems.

Using the exact analytical results, we examined nonequilibrium thermodynamics as a general framework, with equilibrium thermodynamics as the limiting case. Equilibrium systems minimize the free energy or maximize the entropy, whereas non-equilibrium systems exhibit irreversible dynamics. This study addresses the following key questions: (1) Can a unified framework, similar to the Boltzmann distribution and Gibbs free energy, be developed for nonequilibrium systems? (2) How is entropy production, a hallmark of irreversibility, quantitatively linked to microscopic processes? (3)

Why do some nonequilibrium systems maximize entropy production while others follow different paths, and can a single principle explain this variability? By addressing these questions, we contribute to our perspective, providing insights into transitions between nonequilibrium and equilibrium, and tools to optimize energy-efficient systems in both natural and engineered environments.

The remainder of this paper is organized as follows: Section 2 examines how the number of accessible states and entropy depend on the model parameters. Section 3 explores the behavior of thermodynamic rates, such as entropy production and extraction rates, as functions of the model parameters. In Section 4, we analyze the velocity, Coefficient of Performance (*COP*) of the refrigerator, and efficiency. Section 5 investigates the temporal evolution of thermodynamic properties in a network of Brownian motors. Finally, Section 6 presents a summary and conclusion.

2. Effective number of accessible states and entropy in nonequilibrium systems

2.1 *Analysis of effective number of accessible states in a ratchet potential with exponential temperature profile*

In this section, we consider a Brownian motor moving along a ratchet potential coupled with an exponentially decreasing thermal arrangement $T(x) = T_h e^{-\alpha x}$, where $\alpha = \dfrac{\ln\left(\dfrac{T_h}{T_c}\right)}{L}$, and periodic for $0 < x < L$. We show that such a thermal arrangement leads to higher velocity, entropy production, and extraction rates compared to the piecewise constant thermal arrangement. By considering discrete thermal and potential arrangements, we solve the master equation and provide an exact time-dependent solution, as detailed in Appendix I. Detailed derivations of thermodynamic quantities, such as entropy, velocity, and entropy production, are presented in Appendix II. It should be noted that such localized temperature variations mimic the temperature distribution of laser-induced heating.

2.2 *Effective number of accessible states*

We now explore the dependence on the number of accessible states. As an alternative approach, the effective number of accessible states, $\Omega_{\text{eff}}(t)$, helps explore the degree of irreversibility. For a given probability distribution $P_i(t)$, we write the effective number of accessible states as

$$\Omega_{\text{eff}}(t) = \prod_{i=1}^{N} P_i(t)^{-P_i(t)}. \tag{1}$$

where N denotes the total number of microstates and $P_i(t)$ represents the probability that the system is in state i at time t. The probabilities satisfy the following normalization condition: $\sum_{i=1}^{N} P_i(t) = 1$, $0 \leq P_i(t) \leq 1$. Accordingly, states with higher probabilities contribute more to $\Omega_{\text{eff}}(t)$, whereas less probable states contribute less. Consequently, $\Omega_{\text{eff}}(t)$ exhibits an effective diversity of microstates. This approach corresponds to the geometric mean of a weighted probability distribution, which serves as an exponential measure based on the logarithmic contributions of $\{P_i(t)\}$.

We calculate the probability distributions $P_i(t)$ in terms of the transition rates using the master equation framework. On the other hand, the Boltzmann entropy (using Equation (1)) is given by

$$S = k_B \ln \Omega_{\text{eff}}(t) = k_B \left(-\sum_{i=1}^{N} P_i(t) \ln P_i(t) \right) \tag{2}$$

where k_B is Boltzmann's constant. The number of accessible states are real and $\Omega_{\text{eff}}(t) \geq 0$. When the system is at equilibrium, all microstates are equally probable, and as a result, one finds $P_i = \frac{1}{N}, \forall i$. For a uniform distribution, $\Omega_{\text{eff}}(t) = N$, which clearly indicates the principle of entropy maximization for equilibrium thermodynamics. Entropy maximization states that systems evolve toward states of maximum entropy, where all accessible microstates are equally probable. At equilibrium, this principle aligns with the minimization of free energy, providing a consistent framework for isolated and closed systems. For our model system (for equilibrium case) in the absence of an external load ($f = 0$), potential ($E = 0$), and with a uniform temperature ($T_h \to T_c$), we find that

$$\Omega_{\text{eff}}(t) = 3\left(1 - e^{-\frac{3t}{2}}\right)^{\frac{2}{3}\left(-1+e^{-\frac{3t}{2}}\right)} \left(1 + 2e^{-\frac{3t}{2}}\right)^{-\frac{1}{3}-\frac{2}{3}e^{-\frac{3t}{2}}}. \tag{3}$$

In the limit $t \to \infty$, this approach approaches $\Omega_{\text{eff}} \approx 3$, which represents maximum entropy. This result is consistent because our ratchet potential is consistent with those of the three lattice sites.

Our analysis indicates that far from equilibrium, the effective number of accessible states $\Omega_{\text{eff}}(t)$ is generally less than the total number of microstates N. These results ensure that $\Omega_{\text{eff}}(t) < N$ under non-equilibrium conditions, with $\Omega_{\text{eff}}(t)$ approaching N only at equilibrium. As illustrated in Figure 1, for systems driven out of equilibrium, $\Omega_{\text{eff}} < 3$. Notably, $\Omega_{\text{eff}}(t)$ is significantly larger for an exponential thermal arrangement than for a piecewise constant-temperature profile. This indicates that systems with exponential thermal arrangements are more irreversible than those with piecewise constant-temperature profiles.

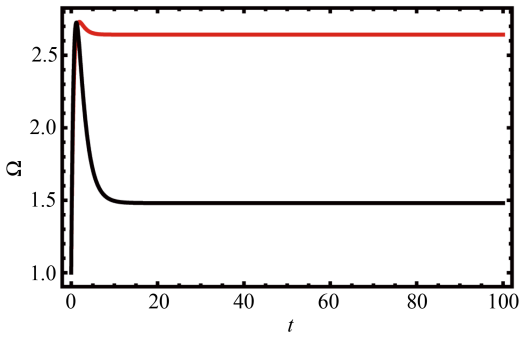

Figure 1. (Color online) The Ω as a function of t and $\tau = 6$ evaluated analytically via Equation (11) for given values of $\varepsilon = 2.0$ and $f = 0.5$. The topmost curve corresponds to an exponential temperature profile, whereas the bottom curve represents a piecewise constant-temperature arrangement. This indicates that a system with an exponential thermal arrangement is more irreversible than a system with a piecewise constant-temperature profile

Hereafter, when plotting the figures, we use the rescaled load $\lambda = f/T_c$, barrier height $\varepsilon = E/T_c$, and dimensionless temperature $\tau = T_h/T_c$. Quantity Ω, as a function of ε and λ, is analytically evaluated using Equation (1) for $t = 100,000.0$ and $\tau = 2.0$ in Figure 2. The uppermost curve corresponds to an exponential temperature profile, whereas the lowermost curve represents a piecewise constant temperature configuration. These results demonstrate that systems with an exponential thermal arrangement exhibit a higher degree of irreversibility than those with a piecewise constant temperature profile.

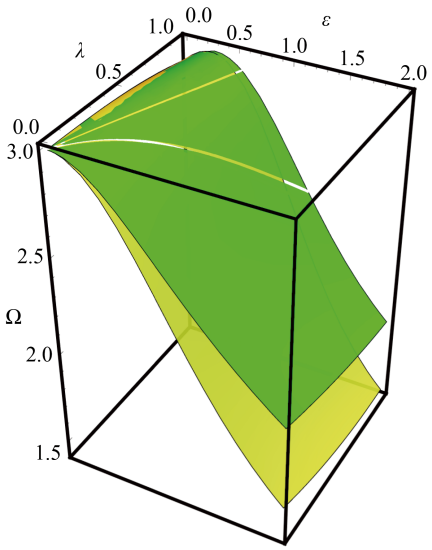

Figure 2. (Color online) The Ω as a function of ε and λ evaluated analytically via Equation (1) for a given $t = 100,000.0$ and $\tau = 2.0$. The topmost curve corresponds to an exponential temperature profile, while the bottom curve represents a piecewise constant temperature arrangement. This reflects that system with exponential thermal arrangement is more irreversible than system with a piecewise constant temperature profile

2.3 *Entropy and free energy in nonequilibrium systems*

We derive the probability distribution as a function of time, load f, and ratchet potential E for an exponentially decreasing temperature gradient that varies from T_h to T_c (see Appendix I). Because the expressions for the probability distributions in the nonequilibrium case are lengthy, we do not present them here. Using these distributions, we calculate key thermodynamic quantities, including the entropy and free energy.

To gain insight into the irreversibility of these processes, we focus on studying entropy production. Using the exact analytical results, we address the critical question of how entropy production can be quantitatively linked to microscopic processes. By employing Gibbs entropy and solving the probability distribution of microstates, we bridge microscopic dynamics with the macroscopic thermodynamic properties. Notably, for systems governed by a master equation, the Boltzmann-Gibbs nonequilibrium entropy and entropy balance equation offer a reliable and robust framework. The Gibbs entropy is given by

$$S(t) = -k_B \sum_i P_i(t) \ln P_i(t), \tag{4}$$

where $P_i(t)$ denotes the probability that the system is in state i at time t. This approach allowed us to compute macroscopic quantities (such as entropy production and entropy flow) directly from microscopic probabilities. Theoretical studies [1–3] have shown that non-equilibrium systems continuously produce and extract entropy. At steady state, the entropy production rate balances the entropy extraction rate. Thus, the dynamics described by Gibbs entropy directly link microscopic stochastic processes with those of macroscopic dynamics, which in turn improves our understanding of irreversibility in non-equilibrium systems.

We now compare the entropy of the exponentially decreasing temperature case with that of piecewise constant thermal arrangements. Figure 3 shows the entropy $S(t)$ as a function of time t and λ for fixed values of $\tau = 2.0$ and $\varepsilon = 2.0$. The results clearly show that the entropy is significantly higher for an exponentially decreasing temperature gradient than for piecewise constant thermal arrangements.

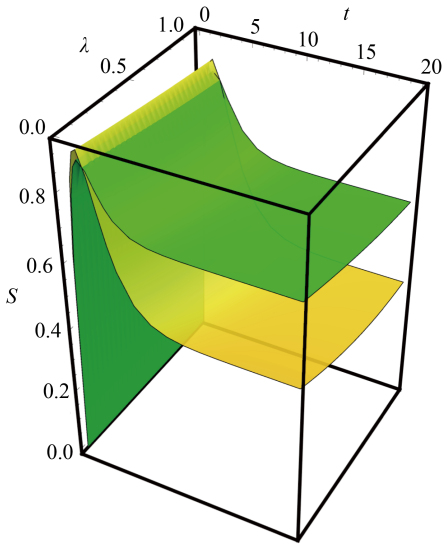

Figure 3. (Color online) Entropy $S(t)$ as a function of time t and λ for fixed $\tau = 2.0$ and $\varepsilon = 2.0$. The top curve represents an exponential temperature profile, whereas the bottom curve corresponds to a piecewise constant arrangement. The results show that the system with the exponential thermal arrangement has a considerably large entropy

In equilibrium systems, principles such as Gibbs free energy provide a well-established framework. Recent studies have suggested that Gibbs entropy also applies to nonequilibrium systems, offering a strong foundation for advancing the understanding of nonequilibrium thermodynamics.

Figure 4 shows the free energy as a function of time, t plotted for $\tau = 6$, $\varepsilon = 2.0$, and $f = 0.5$. The top curve represents the exponential thermal arrangement, whereas the bottom curve corresponds to the piecewise constant-temperature case.

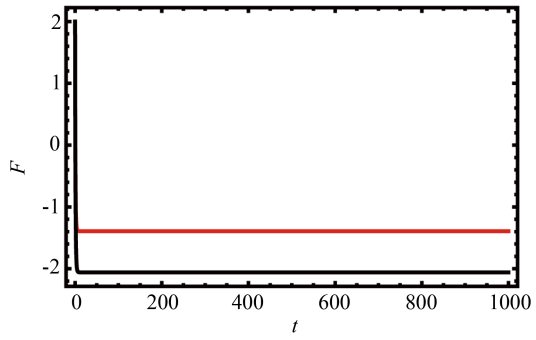

Figure 4. (Color online) The free energy as a function of t, with $\tau = 6$, is plotted for a fixed $\varepsilon = 2.0$ and $f = 0.5$. The top curve represents the exponential temperature case, whereas the bottom curve corresponds to the piecewise constant-temperature case

To gain a better understanding of the system, we analyze specific limiting cases. First, we consider the isothermal case, where $T_h \to T_c$ and $f \to 0$. Under steady-state conditions, entropy S can be expanded to small barrier heights E as

$$S = \ln[3] - \frac{E^2}{3T_c^2} + \frac{E^4}{12T_c^4}. \tag{5}$$

From this expression, it is clear that as $E \to 0$, the system approaches equilibrium, and the entropy reduces to $S = \ln[3]$, which is the expected value at equilibrium. In the absence of ratchet potential, the system achieves maximum entropy. This

also implies that when the system reaches equilibrium, it signifies that it obeys the detailed balance condition, meaning that the probability flux between any pair of states becomes symmetric and net currents vanish. Conversely, for a small but nonzero E, the system deviates slightly from equilibrium, with entropy corrections proportional to E^2 and higher-order terms.

Next, we consider the isothermal case with a nonzero force, where $E = 0$ and the system is driven out of equilibrium by an external load, f. Under steady-state conditions, expanding S to a small f yields

$$S = \ln[3] - \frac{f^4}{27T_c^4} + \frac{f^5}{81T_c^5}. \tag{6}$$

In this case, when $f \to 0$, the entropy decreases to $S = \ln[3]$, corresponding to the equilibrium. However, for any nonzero f, the system is driven out of equilibrium, resulting in an increase in entropy. This demonstrates that an external force alone, even in the absence of a potential, can generate non-equilibrium dynamics. These two limiting cases highlight the role of the potential barrier and external force in driving the system out of non-equilibrium states. While the system approaches equilibrium when E or f tends to zero, small expansions in these parameters reveal how they influence the entropy dynamics and deviations from equilibrium.

We emphasize that the principle of entropy maximization is fundamental to equilibrium thermodynamics. This principle states that systems evolve toward maximum entropy, where all microstates are equally probable. At equilibrium, this is directly linked to free-energy minimization, forming a consistent framework for isolated and closed systems. In contrast, nonequilibrium systems display more complex behaviors, with entropy production influenced by external forces, thermal gradients, and nonlinearities. As nonequilibrium thermodynamics extend beyond equilibrium conditions, entropy maximization is only a special case. As shown earlier, entropy maximizes or free energy is minimized only under a uniform probability distribution, $P_i(t) = 1/N$ for all i, a condition that applies exclusively at equilibrium.

This can be appreciated when one writes the probabilities as a function of time for the equilibrium and isothermal cases. In the absence of a potential barrier ($E = 0$), load ($f = d = 0$) and when ($t \to \infty$), we get the free energy

$$F = -T_c \ln(3) \tag{7}$$

which is the free energy of the three-state system presented in this study.

This result can be verified using a statistical mechanical approach. In the limit $t \to \infty$, the probability distributions (shown in Appendix I) converge

$$P_1 = \frac{1}{1 + e^{-E/T_c} + e^{-2E/T_c}} \tag{8}$$

$$P_2 = \frac{e^{-E/T_c}}{1 + e^{-E/T_c} + e^{-2E/T_c}} \tag{9}$$

$$P_3 = \frac{e^{-2E/T_c}}{1 + e^{-E/T_c} + e^{-2E/T_c}} \tag{10}$$

The partition function is given

$$Z = \sum_{i=1}^{3} e^{-E_i/T_c} = 1 + e^{-E/T_c} + e^{-2E/T_c}. \tag{11}$$

Using Z, the free energy and entropy are calculated as

$$F = -T_c \ln(Z), \quad S = \ln(Z) + \bar{E}\beta, \tag{12}$$

where $\bar{E}$ represents the average energy and $\beta = 1/T_c$.

In the limit $E \to 0$, the partition function is simplified to $Z = 3$. Consequently, the free energy converges to

$$F = -T_c \ln(3), \tag{13}$$

and entropy approaches:

$$S = \ln(3). \tag{14}$$

These results confirm the consistency of the thermodynamic relationships in the isothermal case at equilibrium. Equivalently, we can directly evaluate entropy S in the absence of a load, $T_h = T_c$ and $E = 0$ as

$$S = \frac{1}{3} e^{-3t/2} \left[-2\left(-1 + e^{3t/2}\right) \ln\left(\frac{1}{3} - \frac{1}{3} e^{-3t/2}\right) - \left(2 + e^{3t/2}\right) \ln\left(\frac{1}{3} + \frac{2}{3} e^{-3t/2}\right) \right]. \tag{15}$$

In the limit $t \to \infty$, the entropy is simplified to

$$S = \ln(3), \tag{16}$$

as expected, since the system has three lattice points.

The above analysis indicates that nonequilibrium thermodynamics encompasses a broader range of conditions than equilibrium; thus, entropy maximization arises only as a limiting case. Thus, it is my perspective that Gibbs entropy provides a universal framework linking microscopic dynamics to macroscopic thermodynamic properties, applicable to both equilibrium and non-equilibrium systems. In nonequilibrium thermodynamics, which encompasses systems with varying thermodynamic fluxes, thermal gradients, and external forces, entropy maximization emerges only as a special limiting case. Systems that are far from equilibrium require individual treatment based on their configuration, because they exhibit unique behavior. This process begins by determining the probability distribution, which forms the foundation for analyzing the thermodynamic properties and understanding the interplay between irreversibility, energy dissipation, and entropy production.

3. Entropy production and extraction rates

In this section, we explore the dependence of several thermodynamic relations, such as entropy production and extraction rates, on the model parameters. The differentiation of the entropy with respect to time leads to

$$\frac{dS_{\text{tot}}}{dt} = \dot{e}_p - \dot{h}_d. \tag{17}$$

Here, $(\dot{e}_p)$ denotes the entropy production rate, and $\dot{h}_d$ denotes the entropy extraction rate. S_{tot} is the total entropy of the system. Because the expressions for the probability distribution and transition rates are obtained analytically, we can write the first and second laws of thermodynamics in terms of the model parameters. This enabled us to uncover several new thermodynamic relations specific to these temperature profiles.

In general, the entropy production and extraction rates were substantially higher for an exponentially decreasing temperature profile than for a piecewise constant thermal arrangement. In Figure 5, the entropy production rate $(\dot{e}_p)$ is plotted as a function of τ and ε for $\lambda = 0.1$. The figure shows that the exponentially decreasing temperature profile exhibits significantly higher entropy, entropy production rate, and velocity than the piecewise constant thermal arrangement.

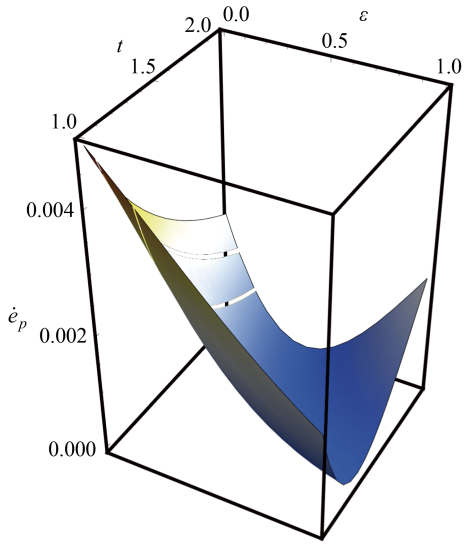

Figure 5. (Color online) Entropy production rate $(\dot{e}_p)$ as a function of τ and ε for a given $\lambda = 0.1$

In Figure 6, we plot the entropy production rate as a function of time. As time progresses, the entropy production rate decreases and approaches a constant value. The figure also shows that the entropy production is significantly higher for the linearly decreasing temperature profile than for the piecewise constant case. In Figure 7, we plot the entropy extraction rate as a function of time, which again demonstrates that the extraction rate is higher in the case of exponentially decreasing temperature. Finally, in Figure 8, we present $\dot{S}$ as a function of time.

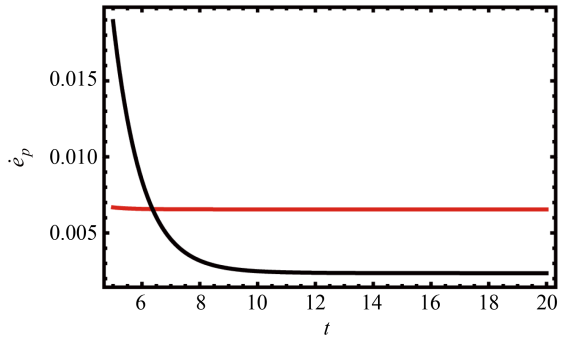

Figure 6. (Color online) Entropy production rate as a function of t for $\tau = 6$, $\varepsilon = 2.0$ and $f = 0.5$. The top curve corresponds to an exponential temperature profile, whereas the bottom curve represents a piecewise constant-temperature arrangement

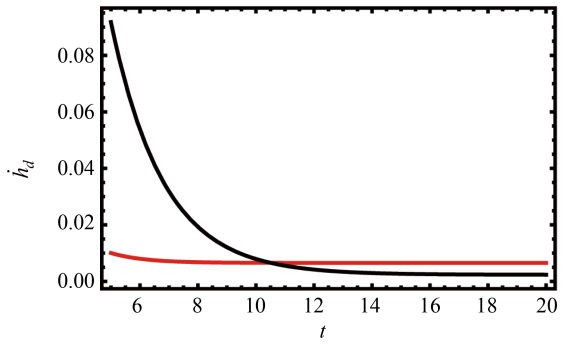

Figure 7. (Color online) The entropy extraction rate is plotted as a function of t for $\tau = 6$, $\varepsilon = 2.0$, and $f = 0.5$. The top curve represents an exponential temperature profile, while the bottom curve corresponds to a piecewise constant temperature arrangement

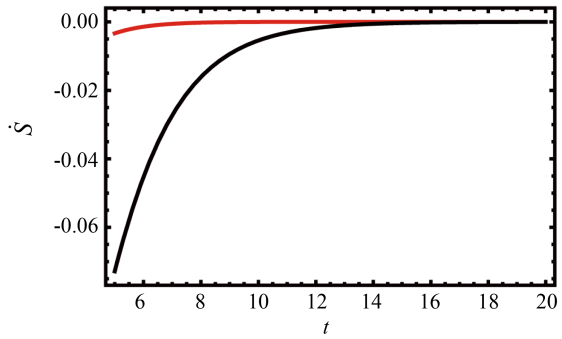

Figure 8. (Color online) The change in entropy is plotted as a function of t for $\tau = 6$, $\varepsilon = 2.0$, and $f = 0.5$. The top curve corresponds to a piecewise constant-temperature arrangement, whereas the bottom curve represents an exponential temperature profile

As the first limiting case, we consider the steady state in the absence of a ratchet potential, where the system remains out of equilibrium due to the external force. Under these conditions, the entropy production rate and heat dissipation rate are given by

$$\dot{e}_p = \dot{h}_d = \frac{3(-1+e^{f/T_c})f}{2(T_c+2e^{f/T_c}T_c)} \tag{18}$$

regardless of the thermal arrangement. As shown, both $\dot{e}_p$ and $\dot{h}_d$ are positive, indicating an irreversible process. In the limit $f \to 0$, we obtain $\dot{e}_p = \dot{h}_d = 0$, which signifies that the system approaches equilibrium.

In the absence load, isothermal case and in the limit $E \to 0$, for all thermal arrangement, we get

$$\dot{e}_p = e^{-\frac{3t}{2}} \left(-\log\left[-1 + e^{\frac{3t}{2}}\right] + \log\left[2 + e^{\frac{3t}{2}}\right] \right) \tag{19}$$

while integrating $\int_0^\infty (\dot{e}_p) dt$ leads to $S = e_p = \ln[3]$.

In an equilibrium system, entropy is determined by the number of accessible microstates. For our three-state system in equilibrium, where each state has an equal probability, the entropy is given by $S = k_B \ln 3$. This represents the maximum entropy for a three-state system at equilibrium, in which no external forces or temperature gradients disturb the system. In our case, we consider a three-state system operating under nonequilibrium conditions, where deviations from equilibrium modify the entropy owing to external influences, such as forces or thermal gradients. Moreover

$$\dot{E}_p = T_c e^{-\frac{3t}{2}} \left(-\log\left[-1 + e^{\frac{3t}{2}}\right] + \log\left[2 + e^{\frac{3t}{2}}\right] \right) \tag{20}$$

while integrating $\int_0^\infty (\dot{E}_p) dt$ leads to $S^T = E_p = T_c \ln[3]$.

4. Velocity and efficiency

Brownian motors with ratchet potentials and spatially varying temperatures can achieve directed motion even without external forces. The thermal asymmetry and applied load generate a net particle current, offering valuable insights into microscale and nanoscale transport systems, in which controlled motion is essential. Notably, adjusting the thermal arrangement alone enables directed motion. By tuning the system parameters, such as barrier height, load, and noise intensity, the particle velocity can be optimized. This, in turn, improves the efficiency of microfluidic devices and nanoscale sensors.

For exponentially decreasing temperature case, after some algebra the velocity is given as

$$V = \frac{3\left(e^{\frac{2E}{T_c}} - e^{\frac{E T_c + f T_c + f T_h + (E+f) T_c \left(\frac{T_h}{T_c}\right)^{1/3}}{T_c T_h}} \right)}{2\left(1 + 2e^{\frac{(E+f)\left(\frac{T_h}{T_c}\right)^{1/3}}{T_h}} \right)\left(e^{\frac{2E}{T_c}} + e^{\frac{E+f}{T_h}} \left(e^{\frac{2E}{T_c}} + e^{\frac{f}{T_c}} \right) \right)}. \tag{21}$$

The stall force at which current becomes zero is given as

$$f' = \frac{-E T_c + 2E T_h - E T_c \left(\frac{T_h}{T_c}\right)^{1/3}}{T_c + T_h + T_c \left(\frac{T_h}{T_c}\right)^{1/3}} \tag{22}$$

The system sustains a nonzero velocity only in the presence of a symmetry-breaking field, such as a nonuniform temperature or an external load. To demonstrate this, we expand Equation (21) for a small force in the absence of a ratchet potential and at a uniform temperature. After some algebra, we obtain

$$V = -\frac{f}{2T_c} + \frac{f^2}{12T_c^2}. \tag{23}$$

Clearly, only in the limit $f \to 0$ does the velocity vanish, indicating that the external force is responsible for the unidirectional motion of the particle.

In the absence of load f, the particle still attains unidirectional motion, but only in the presence of a ratchet potential and non-uniform thermal arrangement. Expanding Equation (21) for a small barrier height E, we obtain

$$V = \frac{1}{6}\left(\frac{2}{T_c} - \frac{1+(T_h/T_c)^{1/3}}{T_h}\right)E^2, \tag{24}$$

In the limit $T_h \to T_c$, the velocity approaches zero, confirming that a unidirectional current arises owing to the thermal asymmetry and ratchet potential.

We now plot the velocity as a function of the key parameters. Velocity, as a function of the model parameters, exhibits patterns similar to those observed in systems with quadratic [36], linear, and piecewise constant [37] thermal arrangements. As shown in Figure 9, for a large load, the current reverses its direction. To compare the velocity between the exponential and piecewise constant-temperature cases, we computed their velocity ratios. Figure 10 shows that the velocity is significantly higher for the exponentially decreasing temperature case.

The motor functions as a heat engine when the external force f is less than the stall force f'. To analyze its performance, we examine its efficiency η. The efficiency of a Brownian motor is defined as the ratio of the useful output work given by $W = 3f$ to the total energy input $E_{\text{in}} = 2E + 2f$. For a system driven by a ratchet potential and thermal gradient, the efficiency in the quasistatic limit is given by

$$\eta = 1 - \frac{T_c\left(1+\left(\frac{T_h}{T_c}\right)^{1/3}\right)}{2T_h}. \tag{25}$$

where T_h and T_c represent the temperatures of the hot and cold reservoirs, respectively. This efficiency is significantly lower than the Carnot efficiency, which represents the theoretical maximum efficiency in the quasistatic limit of a piecewise constant-temperature system.

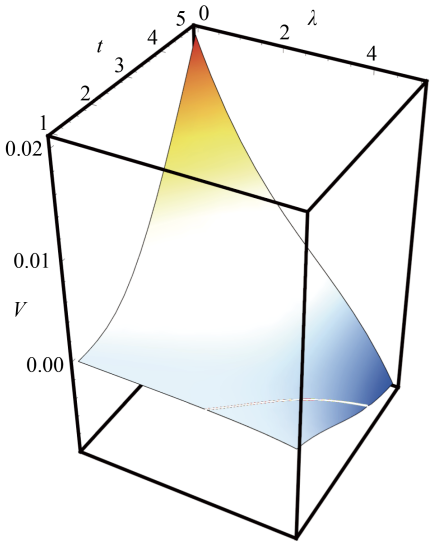

Figure 9. (Color online) The velocity as a function of τ and λ evaluated analytically for a given $\varepsilon = 6.0$

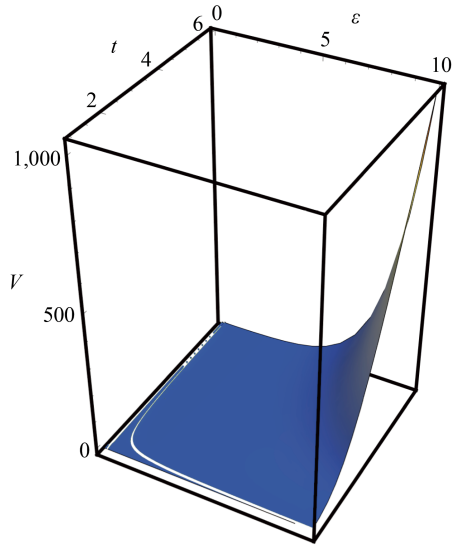

Figure 10. (Color online) The ratio of the velocity between the exponential decreasing and piecewise constant temperature cases is evaluated analytically as a function of τ and ε for a given $\lambda = 0.1$. The results highlight that the efficiency of the exponential temperature case is considerably higher than that of the piecewise constant-temperature case

A key observation is that Brownian motors operating under an exponentially decreasing temperature profile generally achieve higher velocities but at the cost of lower efficiency compared to piecewise constant thermal arrangements. In contrast, motors operating under linearly or quadratically varying temperature profiles exhibit very high velocities but lower efficiencies, reflecting the trade-off between speed and energy conversion efficiency.

When $f > f'$, the motor transitions to refrigeration mode, where it pumps heat against the thermal gradient. The Coefficient of Performance (COP) is defined as the ratio of heat extracted from the cold reservoir, $Q_{\text{cold}} = 2E - f$, to the work input, $W_{\text{input}} = 3f$. In the quasistatic limit, the COP is given by

$$COP = -\frac{T_c\left(1+\left(\frac{T_h}{T_c}\right)^{1/3}\right)}{T_c - 2T_h + T_c\left(\frac{T_h}{T_c}\right)^{1/3}}. \tag{26}$$

While calculating the efficiency and the Coefficient of Performance (*COP*), we assume periodic boundary conditions and a continuous, exponentially varying temperature field along the spatial coordinate.

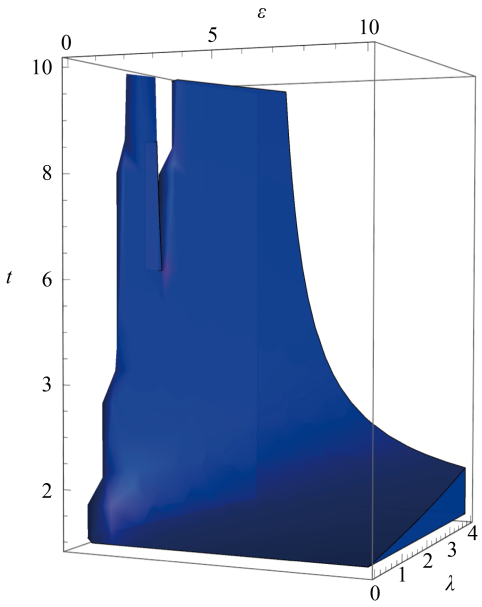

Figure 11. (Color online) The phase diagram illustrates the regime where the engine operates as a refrigerator, plotted as a function of ε, λ, and τ. This diagram provides insight into the parameter space in which the motor transitions from the heat engine mode to the refrigeration mode, highlighting the dependence of performance on system characteristics

The phase diagram shown in Figure 11 illustrates the regime in which the engine operates as a refrigerator, plotted as a function of ε, λ, and τ. This diagram provides insight into the parameter space in which the motor transitions from heat engine mode to refrigeration mode, highlighting the dependence of performance on system characteristics.

Our analysis reveals that Brownian motors operating under an exponentially decreasing temperature gradient generally exhibit a lower *COP* than those operating in a piecewise constant thermal environment. This is because a continuously varying temperature gradient leads to additional entropy production, thereby increasing the energy dissipation. However, these motors still offer advantages in terms of enhanced velocity, making them suitable for applications in nanoscale energy harvesting and transportation [36]. For instance such motors have promising applications across a range of nanoscale technologies. In biological systems, molecular machines such as kinesin and dynein harness stochastic forces to transport cellular cargo with directionality and efficiency, offering a natural template for synthetic analogs. Inspired by these mechanisms, artificial Brownian motors can be integrated into nanoscale energy harvesting platforms and autonomous micro-carriers for targeted drug delivery, where enhanced velocity and rectification are crucial. Moreover, in microfluidic environments, noise-assisted transport can be exploited for the design of Brownian pumps and particle-sorting devices, enabling controlled motion without macroscopic gradients. These applications illustrate the technological potential of nonequilibrium-driven transport systems in both biomedical and soft-matter engineering contexts.

5. Brownian particle dynamics in a network of M ratchet potentials

In this study, we consider a Brownian particle moving in a network. We show that, similar to our previous study [36], the rates of thermodynamic quantities such as velocity, entropy production rate, and entropy extraction rate are independent of network size at steady state. However, extensive properties such as entropy, entropy production, and entropy extraction increase with network size, even in the steady state. We will then compare these thermodynamic relations with systems operating between hot and cold baths and those where the temperature decreases exponentially along the reaction coordinate.

Master's equation approach. One can directly calculate the thermodynamic relations. For instance, the dynamics of a Brownian particle moving within a network of two ratchet potentials can be described by considering a periodic boundary condition as

$$\frac{dp_1(t)}{dt} = P_{1,\,2}p_2 - P_{2,\,1}p_1 + P_{1,\,3}p_3 - P_{3,\,1}p_1 \tag{27}$$

$$\frac{dp_2(t)}{dt} = P_{2,\,1}p_1 - P_{1,\,2}p_2 + P_{2,\,3}p_3 - P_{3,\,2}p_2 \tag{28}$$

$$\frac{dp_2(t)}{dt} = P_{2,\,1}p_1 - P_{1,\,2}p_2 + P_{2,\,3}p_3 - P_{3,\,2}p_2 \tag{29}$$

$$\frac{dp_3(t)}{dt} = P_{3,\,2}p_2 - P_{2,\,3}p_3 + P_{3,\,1}p_1 - P_{1,\,3}p_3 \tag{30}$$

$$\frac{dp_3(t)}{dt} = P_{3,\,2}p_2 - P_{2,\,3}p_3 + P_{3,\,1}p_1 - P_{1,\,3}p_3 \tag{31}$$

The above differential equations can be simplified to

$$\frac{dp_1(t)}{dt} = P_{1,\,2}p_2 - P_{2,\,1}p_1 + P_{1,\,3}p_3 - P_{3,\,1}p_1 \tag{32}$$

$$\frac{dp_2(t)}{dt} = P_{2,\,1}p_1 - P_{1,\,2}p_2 + P_{2,\,3}p_3 - P_{3,\,2}p_2 \tag{33}$$

$$\frac{dp_3(t)}{dt} = P_{3,\,2}p_2 - P_{2,\,3}p_3 + P_{3,\,1}p_1 - P_{1,\,3}p_3 \tag{34}$$

Note that even though the above differential equations are reduced to three equations, entropy does not simplify in the same way. The total entropy depends on the number of sites in the network. For a network consisting of N sites, the entropy S is expressed as

$$S = -k_B \sum_{i=1}^{N} P_i(t) \ln P_i(t), \tag{35}$$

where $P_i(t)$ represents the probability that a particle occupies state i at time t. This dependency arises because entropy is an extensive quantity that depends on the number of microstates in the system. While dynamical rates, such as velocity, entropy production rate, and entropy extraction rate, are independent of network size, the total entropy grows proportionally with the number of sites, reflecting the increasing complexity of the system. For instance, for any network size M, at steady state we find the velocity

$$V = \frac{3\left(e^{\frac{2E}{T_c}} - e^{\frac{E T_c + f T_c + f T_h + (E+f) T_c \left(\frac{T_h}{T_c}\right)^{1/3}}{T_c T_h}}\right)}{2\left(1 + 2e^{\frac{(E+f)\left(\frac{T_h}{T_c}\right)^{1/3}}{T_h}}\right)\left(e^{\frac{2E}{T_c}} + e^{\frac{E+f}{T_h}}\left(e^{\frac{2E}{T_c}} + e^{\frac{f}{T_c}}\right)\right)}. \tag{36}$$

The stall force at which current becomes is given as

$$f = \frac{-E T_c + 2E T_h - E T_c \left(\frac{T_h}{T_c}\right)^{1/3}}{T_c + T_h + T_c \left(\frac{T_h}{T_c}\right)^{1/3}} \tag{37}$$

Because the rate equations are independent of the network size M, their expressions have already been discussed in the previous section. Here, we further investigate extensive quantities, such as entropy, as a function of the model parameters. Because the probability for each lattice site is exactly obtained as a function of the model parameters, we can construct a complete picture of S. However, its expression is too complex to be presented here. Instead, to provide insight for readers, we explore some key limiting cases. We now explore the entropy for $M = 4$ (four Brownian particles arranged in a network sharing the same endpoint with periodic boundary conditions).

For the isothermal case (at steady state) and in the absence of a ratchet potential, expanding S for small f gives

$$S = \ln[9] - \frac{2f^4}{81T_c^4}. \tag{38}$$

In the limit $f \to 0$, entropy approaches $S \to \ln[9]$, as expected.

Similarly, in the absence of load (at steady state) and under isothermal conditions, expanding S for small E yields

$$S = \ln[9] - \frac{2E^2}{9T_c^2}. \tag{39}$$

Once again, in the limit $E \to 0$, the entropy converges to $S \to \ln[9]$, confirming the expected equilibrium behavior. Care must be taken here: for $M = 1$, the entropy is $S = \ln[3]$; for $M = 2$, it is $S = \ln[5]$; and for $M = 4$, it is $S = \ln[9]$. This is because these repetitive network structures share the same nodes at both ends. As shown in Figure 13, for $M = 2$, the system consists of five lattice sites.

Generating Function Approach. In this section, we demonstrate that the rate of thermodynamic relations remains independent of the network size M at steady state, adapting the mathematical approach introduced by Goldhirsch *et al.* [38, 39]. This methodology was also employed in our recent work to compute the motor velocity [36].

For clarity, we first review the underlying mathematical techniques. Consider a segment with sites $0,\ 1,\ 2,\ \ldots,\ N$. Let $P_{2,\ 1}$ denote the probability per unit time step for the walker to transition from site 1 to 2 and $P_{1,\ 2}$ denote the probability for the reverse transition, subject to the condition $P_{1,\ 2} + P_{2,\ 1} \leq 1$. Probability $P_w(n)^+$ represents the likelihood that the walker starts at $j = 0$ and reaches $j = N$ in n steps in the rightward direction.

The Mean First Passage Time (MFPT) to reach $j = N$ is given by

$$\left\langle t^+ \right\rangle = \frac{\sum_{n=0}^{\infty} nP_w(n)^+}{\sum_{n=0}^{\infty} P_w(n)^+}. \tag{40}$$

The corresponding generating function in terms of parameter ϕ is expressed as

$$G_N(\phi)^+ = \sum_{n=0}^{\infty} e^{i\phi n} P_w(n)^+, \tag{41}$$

where $0 < \phi < 2\pi$. The MFPT can then be rewritten in terms of the generating function as

$$t^+ = \frac{d}{d(i\phi)} G_N(\phi)^+ \bigg|_{\phi=0}. \tag{42}$$

The probabilities $P_1,\ P_2,\ \ldots$ can be represented in terms of ϕ as $P_1 e^{i\phi},\ P_2 e^{i\phi},\ \ldots$. The probability that the walker remains at $j = 0$ after n steps is $(1 - P_1)^n$, and the generating function is given by

$$X_{1-P_{1,\ 2}} = \sum_{n=0}^{\infty} (1 - P_{1,\ 2})^n e^{i\phi n} = \frac{1}{1 - (1 - P_1)e^{i\phi}}. \tag{43}$$

Similarly, the probability of remaining at site j for n steps is

$$X_{1-P_{1,\ 2}-P_{2,\ 1}} = \sum_{n=0}^{\infty} (1 - P_{1,\ 2} - P_{2,\ 1})^n e^{i\phi n} = \frac{1}{1 - (1 - P_{1,\ 2} - P_{2,\ 1})e^{i\phi}} \tag{44}$$

The probability of reaching $j = N$ without returning to $j = 0$ is defined by the generating function

$$T_N^+ = \sum_{n=0}^{\infty} e^{i\phi n} U(n)^+, \tag{45}$$

whereas the probability of returning to $j = 0$ without reaching $j = N$ is given by

$$Q_N(\phi)^+ = \sum_{n=0}^{\infty} e^{i\phi n} V(n)^+. \tag{46}$$

Through recursive iterations, the generating function for the first passage time is formulated as

$$G_N(\phi)^+ = \frac{X_{1-P_{1,\,2}} T_N^+}{1 - X_{1-P_{1,\,2}} Q_N^+(\phi)}, \tag{47}$$

For a Brownian particle navigating a complex network, the MFPT generating function in the right direction is

$$G_M(\phi)^+ = \frac{X'_{1-P_{1,\,2}}(T_1^+ + \cdots + T_M^+)}{1 - X'_{1-P_{1,\,2}}(Q_1^+ + \cdots + Q_M^+)}. \tag{48}$$

Because the networks exhibit repetitive behavior, the expression $X'_{1-P_{1,\,2}}$ can be written as $X_{1-P_{1,\,2}}/M$. Moreover, the summation of the terms $(T_1^+ + \cdots + T_M^+)$ simplifies to MT_N^+, and similarly, $(Q_1^+ + \cdots + Q_M)$ results in MQ_N. Consequently, Equations (35) and (36) are found to be exactly equivalent, which demonstrates that the velocity and other thermodynamic rates are independent of the lattice size M. Following similar steps, the left-direction generating function takes the form

$$G_M(\phi)^- = \frac{X'_{1-P_{3,\,1}}(T_1^- + \cdots + T_M^-)}{1 - X'_{1-P_{3,\,1}}(Q_1^- + \cdots + Q_M^-)}. \tag{49}$$

Considering M identical potentials, the net average velocity, independent of the lattice size M, simplifies to

$$V \approx \frac{3\left(e^{\frac{2E}{T_c}} - e^{\frac{E,\ T_c+f,\ T_c+f,\ T_h+(E+f),\ T_c,\ \left(\frac{T_h}{T_c}\right)^{1/3}}{T_c,\ T_h}}\right)}{2\left(1+2,\ e^{\frac{(E+f),\ \left(\frac{T_h}{T_c}\right)^{1/3}}{T_h}}\right)\left(e^{\frac{2E}{T_c}} + e^{\frac{E+f}{T_h}}\left(e^{\frac{2E}{T_c}} + e^{\frac{f}{T_c}}\right)\right)}. \tag{50}$$

Using the method of generating functions, we demonstrate that the rates, such as the velocity, are independent of the number of lattice sites.

6. Summary and conclusion

In this study, we explore the dependence of several thermodynamic relationships for a Brownian particle that walks in ratchet potential, coupled with an exponentially decreasing temperature profile. Such a thermal arrangement mimics localized heating, in which the temperature decreases spatially. Our exact analytical solutions show that the velocity, entropy production, and extraction rates are significantly higher than those observed in piecewise constant thermal arrangements.

Moreover, we also analyze the thermodynamic behavior of Brownian particles in the networks. The analytical results indicate that the relationships between thermodynamic rates, such as the velocity and entropy production rate, remain independent of the network size. However, extensive quantities, such as total entropy, depend on the number of microstates. The analytical results also indicate that a system with an exponentially decreasing temperature gradient exhibits lower entropy production and extraction rates than systems with linearly or quadratically varying thermal gradients.

Furthermore, we show that a Brownian particle that walks in a ratchet potential coupled with a spatially varying temperature achieves directed motion, even without external forces. Symmetry-breaking fields, such as thermal asymmetry and external forces, generate unidirectional motion. The magnitude and direction of particle motion can be adjusted by varying the system parameters, such as barrier height, load, and noise intensity. Thus, the study presented in this work helps improve the efficiency of microfluidic devices and nanoscale sensors by deepening our understanding of thermally driven ratchets and the role of temperature asymmetry in Brownian motors.

We also investigate the relationship between the efficiency and Coefficient of Performance (*COP*) for different thermal arrangements. We show that Brownian motors operating under an exponentially decreasing temperature gradient generally have a lower efficiency than those with piecewise constant thermal profiles. However, these motors achieve higher velocities. Compared with the linearly or quadratically varying thermal arrangement cases, the exponential thermal arrangement yields a higher efficiency but reduced speed.

Using the exact analytical results, we examine nonequilibrium thermodynamics as a general framework, with equilibrium thermodynamics emerging as a special limiting case. We show that equilibrium systems minimize the free energy or maximize the entropy, whereas non-equilibrium systems exhibit irreversible dynamics. This study addresses the following fundamental questions: (1) Can a unified framework, similar to the Boltzmann distribution and Gibbs free energy, be developed for nonequilibrium systems? (2) How is entropy production, a key measure of irreversibility, quantitatively linked to microscopic processes? (3) Why do some nonequilibrium systems maximize entropy production while others follow different paths, and can a unifying principle explain this variability?

By addressing these questions, we provide insights into the transitions between non-equilibrium and equilibrium systems, offering tools to optimize energy-efficient processes in both natural and engineered environments. Future research should extend these findings to systems with many interacting particles, investigate collective dynamics, and validate theoretical predictions through experimental studies. In conclusion, this study advances the understanding of nonequilibrium thermodynamics by deriving thermodynamic relations for a heat engine operating under an exponentially decreasing temperature profile. This setup provides key insights into entropy production, energy dissipation, and transport dynamics. Notably, such a thermal arrangement mimics real-world heating scenarios, such as laser-induced thermal gradients.

Acknowledgement

I would like to thank Mulu Zebene for their constant encouragement.

Data Availability statement

This manuscript has no associated data, or the data will not be deposited. [Authors' comment: Since we presented an analytical work, we did not collect any data from simulations or experimental observations].

Conflict of interest

The author declares that there is no conflict of interests regarding the publication of this paper.

References

[1] Ge H, Qian H. Physical origins of entropy production, free energy dissipation, and their mathematical representations. *Physical Review E*. 2010; 81: 51133.

[2] Tome T, Oliveira MJ. Entropy production in nonequilibrium systems at stationary states. *Physical Review Letters*. 2012; 108: 20601.

[3] Schnakenberg J. Network theory of microscopic and macroscopic behavior of master equation systems. *Reviews of Modern Physics*. 1976; 48: 571.
[4] Tome T, Oliveira MJ. Entropy production in irreversible systems described by a Fokker-Planck equation. *Physical Review E*. 2010; 82: 21120.
[5] Zia RKP, Schmittmann B. Probability currents as principal characteristics in the statistical mechanics of nonequilibrium steady states. *Journal of Statistical Mechanics: Theory and Experiment*. 2007; 7: 7012.
[6] Seifert U. Entropy production along a stochastic trajectory and an integral fluctuation theorem. *Physical Review Letters*. 2005; 95: 40602.
[7] Tome T. Entropy production in nonequilibrium systems described by a Fokker-Planck equation. *Brazilian Journal of Physics*. 2006; 36: 1285.
[8] Szabo G, Tome T, Borsos I. Probability currents and entropy production in nonequilibrium lattice systems. *Physical Review E*. 2010; 82: 11105.
[9] Gaveau B, Moreau M, Schulman LS. Generalized Clausius relation and power dissipation in nonequilibrium stochastic systems. *Physical Review E*. 2009; 79: 10102.
[10] Lebowitz JL, Spohn H. A Gallavotti-Cohen-type symmetry in the large deviation functional for stochastic dynamics. *Journal of Statistical Physics*. 1999; 95: 333.
[11] Andrieux D, Gaspar P. Fluctuation theorem for currents and Schnakenberg network theory. *Journal of Statistical Physics*. 2007; 127: 107.
[12] Harris RJ, Schutz GM. Fluctuation theorems for stochastic dynamics. *Journal of Statistical Mechanics: Theory and Experiment*. 2007; 7: 7020.
[13] Tome T, de Oliveira MJ. Stochastic approach to equilibrium and nonequilibrium thermodynamics. *Physical Review E*. 2015; 91: 42140.
[14] Luo JL, Van den Broeck C, Nicolis G. Stability criteria and fluctuations around nonequilibrium states. *Zeitschrift für Physik B*. 1984; 56: 165.
[15] Mou CY, Luo JL, Nicolis G. Stochastic thermodynamics of nonequilibrium steady states in chemical reaction systems. *Journal of Chemical Physics*. 1986; 84: 7011.
[16] Maes C, Netocny K. Time-reversal and entropy. *Journal of Statistical Physics*. 2003; 110: 269.
[17] Crochik L, Tome T. Entropy production in the majority-vote model. *Physical Review E*. 2005; 72: 57103.
[18] Asfaw M. Thermodynamic feature of a Brownian heat engine operating between two heat baths. *Physical Review E*. 2014; 89: 12143.
[19] Asfaw M. Exact analytical thermodynamic expressions for a Brownian heat engine. *Physical Review E*. 2015; 92: 32126.
[20] Brandner K, Bauer M, Schmid M, Seifert U. Coherence-enhanced efficiency of feedback-driven quantum engines. *New Journal of Physics*. 2015; 17: 65006.
[21] Gaveau B, Moreau M, Schulman LS. Constrained maximal power in small engines. *Physical Review E*. 2010; 82: 51109.
[22] Boukobza E, Tannor DJ. Three-level systems as amplifiers and attenuators: A thermodynamic analysis. *Physical Review Letters*. 2007; 98: 240601.
[23] Taye MA. Free energy and entropy production rate for a Brownian particle that walks on overdamped medium. *Physical Review E*. 2016; 94: 32111.
[24] Taye MA. Entropy production and entropy extraction rates for a Brownian particle that walks in underdamped medium. *Physical Review E*. 2020; 101: 12131.
[25] Ge H. Time reversibility and nonequilibrium thermodynamics of second-order stochastic processes. *Physical Review E*. 2014; 89: 22127.
[26] Lee HK, Kwon C, Park H. Fluctuation theorems and entropy production with odd-parity variables. *Physical Review Letters*. 2013; 110: 50602.
[27] Spinney RE, Ford IJ. Nonequilibrium Thermodynamics of stochastic systems with odd and even variables. *Physical Review Letters*. 2012; 108: 170603.
[28] Lee HK, Kwon C, Park H. Fluctuation theorems and entropy production with odd-parity variables. *Physical Review Letters*. 2013; 110: 50602.
[29] Celani A, Bo S, Eichhorn R. Anomalous thermodynamics at the microscale. *Physical Review Letters*. 2012; 109: 260603.

[30] Manikandan SK, Gupta D, Krishnamurthy S. Inferring entropy production from short experiments. *Physical Review Letters*. 2020; 124: 120603.
[31] Skinner DJ, Dunkel J. Estimating entropy production from waiting time distributions. *Physical Review Letters*. 2021; 127: 198101.
[32] Otsubo S, Ito S, Dechant A, Sagawa T. Estimating entropy production by machine learning of short-time fluctuating currents. *Physical Review E*. 2020; 101: 62106.
[33] Vu TV, Vo VT, Hasegawa Y. Entropy production estimation with optimal current. *Physical Review E*. 2020; 101: 42138.
[34] Koyuk T, Seifert U. Operationally accessible bounds on fluctuations and entropy production in periodically driven systems. *Physical Review Letters*. 2019; 122: 230601.
[35] Strasberg P, Esposito M. Non-Markovian entropy production. *Physical Review E*. 2019; 99: 12120.
[36] Taye MA. Exact time-dependent thermodynamic relations for a Brownian particle moving in a ratchet potential coupled with quadratically decreasing temperature. *Physical Review E*. 2024; 110: 54105.
[37] Taye MA. Exact time-dependent analytical solutions for entropy production rate in a system operating in a heat bath in which temperature varies linearly in space. *Physical Review E*. 2022; 105: 54126.
[38] Goldhirsch I, Gefen Y. Analytic properties of random walks on networks. *Physical Review A*. 1986; 33: 2583.
[39] Goldhirsch I, Gefen Y. Biased random walks on networks. *Physical Review A*. 1987; 35: 1317.

Appendix I

To gain insight into the behavior of a Brownian particle operating between hot and cold thermal baths, we derive its probability distribution in Figure 12. The thermodynamic properties of a system with an exponentially decreasing temperature profile are compared to those of a Brownian particle in a piecewise constant thermal arrangement, as follows:

$$T_j = T_h, \text{ for site } j = 0 \tag{51}$$

$$T_j = T_c, \text{ for sites } j = 1 \text{ and } j = 2 \tag{52}$$

For the exponentially decreasing temperature profile case, the temperature at site i can be expressed as

$$T_i = T_h e^{-\alpha i}, \tag{53}$$

where α is given by

$$\alpha = \frac{\ln\left(\frac{T_h}{T_c}\right)}{3} \tag{54}$$

and i runs from $i = 0$ to $i = 2$.

Here, T_h and T_c are the temperatures of the hot and cold baths, respectively. x_i denotes the position.

The dynamics of a particle moving from one lattice site to the next are assumed to occur randomly. The probability of this transition is governed by the energy barrier that the particle must overcome and the temperature of the coupled thermal reservoir. Specifically, the transition rate per unit time for the particle to jump from site i to $i+1$ is given by

$$\Gamma e^{-\frac{\Delta E}{T_i}}, \tag{55}$$

where $\Delta E = U_{i+1} - U_i$ and Γ represents the attempt frequency of the particle per unit time. Here, Boltzmann's constant k_B and Γ are taken to be unity. During each jump attempt, the particle first determines the direction of movement, either left or right, with equal probability. This jump is governed by the Metropolis algorithm [36]. If $\Delta E \leq 0$, the jump occurs with certainty; otherwise, if $\Delta E > 0$, the jump occurs with probability

$$\exp\left(-\frac{\Delta E}{T_i}\right). \tag{56}$$

The dynamics of a Brownian particle moving within a network (in the presence of load f) can be described by the Master equation:

$$\frac{dp_n}{dt} = \sum_{n \neq n'} \left(P_{nn'} p_{n'} - P_{n'n} p_n\right), n,\ n' = 1,\ 2,\ 3. \tag{57}$$

Please note that the analytical solution incorporates spatial coupling through temperature-dependent transition rates that vary with position according to an exponential profile. These rates follow the Metropolis rule, where the local temperature directly influences the probability of overcoming energy barriers in the ratchet potential. While a full multiplicative noise Langevin framework is not explicitly used, the master equation approach effectively captures its effects via position-dependent stochastic dynamics.

For a single ratchet potential case $M = 1$, considering a periodic boundary condition, one can express Equation (56) as

$$\frac{dp_1(t)}{dt} = P_{1,\,2}p_2 - P_{2,\,1}p_1 + P_{1,\,3}p_3 - P_{3,\,1}p_1 \tag{58}$$

$$\frac{dp_2(t)}{dt} = P_{2,\,1}p_1 - P_{1,\,2}p_2 + P_{2,\,3}p_3 - P_{3,\,2}p_2 \tag{59}$$

$$\frac{dp_3(t)}{dt} = P_{3,\,2}p_2 - P_{2,\,3}p_3 + P_{3,\,1}p_1 - P_{1,\,3}p_3 \tag{60}$$

Here, $P_{n'n}$ is given by the Metropolis rule. For example, $P_{21} = \frac{1}{2}e^{-\frac{E+f}{t1}} = \frac{\mu a}{2}$, $P_{12} = \frac{1}{2}$, $P_{32} = \frac{1}{2}e^{-\frac{E+f}{t2}} = \frac{\nu b}{2}$, $P_{23} = \frac{1}{2}$, $P_{13} = \frac{1}{2}e^{-\frac{2E-f}{t3}} = \frac{\mu^2}{2a}$, $P_{31} = \frac{1}{2}$, where $\mu = e^{-\frac{E}{t1}}$, $\nu = e^{-\frac{E}{t2}}$, $a = e^{-\frac{f}{t1}}$ and $b = e^{-\frac{f}{t2}}$. Here $t_1 = T_h$, $t_2 = T_i = T_h e^{-\alpha}$ and $t_3 = T_c$.

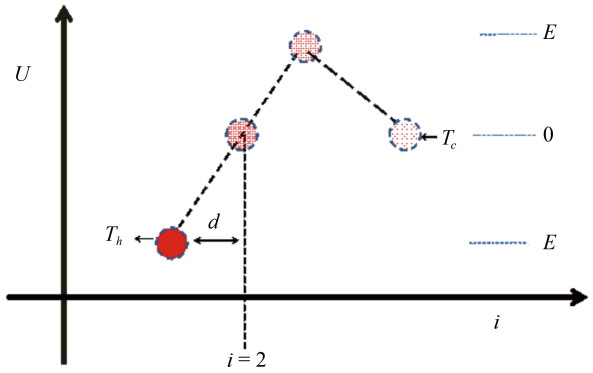

Figure 12. (Color online) The schematic diagram for a Brownian particle that walks in a discrete ratchet potential coupled with a exponentially decreasing temperature heat bath. The temperature of the heat bath decreases from T_h to T_c according to Equation (51)

The above equation can be rewritten in the form $\frac{d\vec{p}}{dt} = \mathbf{P}\vec{p}$. $\mathbf{P}$ has a form

$$\mathbf{P} = \begin{pmatrix} \frac{-\mu_1 a_1}{2} - \frac{\mu_2^2}{2a_2} & \frac{1}{2} & \frac{1}{2} \\ \frac{\mu_1 a_1}{2} & \frac{-1-\nu b}{2} & \frac{1}{2} \\ \frac{\mu_2^2}{2a_2} & \frac{\nu b}{2} & -1 \end{pmatrix}. \tag{61}$$

For a particle that is initially situated at site $i = 2$, the time dependent normalized probability distributions after solving Equation (56) are given as

$$p_1(t) = c_1 \frac{a(2+\nu b)}{\mu\left(\mu + \left(a^2+\mu\right)\nu b\right)} + c_2 e^{-\frac{\left(a+a^2\mu+\mu^2\right)t}{2a}} \left(-1 + \frac{a(-1+a\mu)}{-\mu^2+a\nu b}\right) \tag{62}$$

$$p_2(t) = -c_3 e^{\frac{1}{2}t(-2-\nu b)} - c_2 \frac{a\, e^{-\frac{\left(a+a^2\mu+\mu^2\right)t}{2a}}(-1+a\mu)}{-\mu^2+a\nu b} + c_1 \frac{\left(2a^2+\mu\right)}{\mu+\left(a^2+\mu\right)\nu b} \tag{63}$$

$$p_3(t) = c_1 + c_2 e^{-\frac{\left(a+a^2\mu+\mu^2\right)t}{2a}} + c_3 e^{\frac{1}{2}t(-2-\nu b)} \tag{64}$$

where

$$c_1 = \frac{\mu\left(\mu + \left(a^2+\mu\right)\nu b\right)}{\left(a+a^2\mu+\mu^2\right)(2+\nu b)} \tag{65}$$

$$c_2 = -\frac{a}{\left(a+a^2\mu+\mu^2\right)\left(-1+\frac{a(-1+a\mu)}{-\mu^2+a\nu b}\right)} \tag{66}$$

$$c_3 = -\frac{\mu\left(\mu+a^2\nu b+\mu\nu b\right)}{\left(a+a^2\mu+\mu^2\right)(2+\nu b)} + \frac{a}{\left(a+a^2\mu+\mu^2\right)\left(-1+\frac{a(-1+a\mu)}{-\mu^2+a\nu b}\right)}. \tag{67}$$

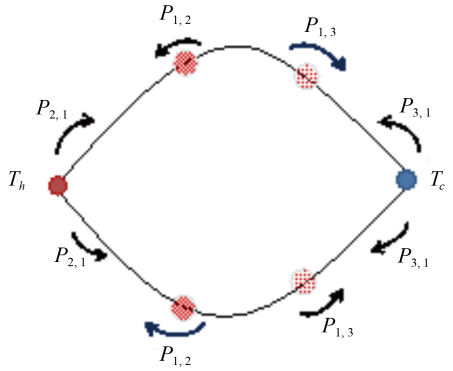

Figure 13. (Color online) The top view that shows two thermal ratchets arranged in a lattice under periodic boundary conditions, where the temperature within each ratchet potential decreases quadratically from the hotter bath (T_h) to the colder bath (T_c). Both ratchet potentials share the same hot and cold baths

Similarly, the dynamics of a Brownian particle moving within a network of two ratchet potentials $M = 2$ can be described by considering a periodic boundary condition as

$$\frac{dp_1(t)}{dt} = P_{1,\,2}p_2 - P_{2,\,1}p_1 + P_{1,\,3}p_3 - P_{3,\,1}p_1 \tag{68}$$

$$\frac{dp_2(t)}{dt} = P_{2,\,1}p_1 - P_{1,\,2}p_2 + P_{2,\,3}p_3 - P_{3,\,2}p_2 \tag{69}$$

$$\frac{dp_3(t)}{dt} = P_{3,\,2}p_2 - P_{2,\,3}p_3 + P_{3,\,1}p_1 - P_{1,\,3}p_3 \tag{70}$$

Here

$$P_{21} = \frac{1}{2}e^{-(E+f)/T_1},\ P_{12} = \frac{1}{2} \tag{71}$$

$$P_{32} = \frac{1}{2}e^{-(E+f)/T_2},\ P_{23} = \frac{1}{2} \tag{72}$$

$$P_{13} = \frac{1}{2},\ P_{31} = \frac{1}{2}e^{-(2E-f)/T_3} \tag{73}$$

Note that the probability distributions are effectively duplicated due to the repetitive network structure, allowing the entropy-related quantities to scale systematically with system size.

The above equation can be rewritten in the form $\frac{d\vec{p}}{dt} = \mathbf{P}\vec{p}$. $\mathbf{P}$ has a form

$$\mathbf{P} = \begin{pmatrix} \frac{-2\mu_1 a_1}{2} - 2\mu_2^2 2a_2 & \frac{1}{2} & \frac{1}{2} & \frac{1}{2} & \frac{1}{2} \\ \frac{\mu_1 a_1}{2} & \frac{-1-\nu b}{2} & 0 & \frac{1}{2} & 0 \\ \frac{\mu_1 a_1}{2} & 0 & \frac{-1-\nu b}{2} & 0 & \frac{1}{2} \\ \frac{\mu_2^2}{2a_2} & \frac{\nu b}{2} & 0 & -1 & 0 \\ \frac{\mu_2^2}{2a_2} & 0 & \frac{\nu b}{2} & 0 & -1 \end{pmatrix} \tag{74}$$

where $\mu_1 = e^{-E/t_1}$, $\nu = e^{-(E+f)/2_2}$, $a_1 = e^{-f/t_1}$, $\mu_2 = e^{-E/t_3}$ and $a_2 = e^{-f/t_3}$.

The expressions for $p_1(t)$, $p_2(t)$, $p_2'(t)$, $p_3(t)$ and $p_3'(t)$ for the particle which is initially situated at site $i = 2$ is given as

$$p_1 = \frac{a_2(2+\nu b)}{a_1 a_2 \mu_1 \nu b + \mu_2^2(1+\nu b)} c_1 + \left(-2 + \frac{2a_2(-1+2a_1\mu_1)}{-2\mu_2^2 + a_2 \nu b}\right) \exp\left[t\left(-\frac{1}{2} - a_1\mu_1 - \frac{\mu_2^2}{a_2}\right)\right] c_3 \tag{75}$$

$$p_2 = \frac{2a_1 a_2 \mu_1 + \mu_2^2}{a_1 a_2 \mu_1 \nu b + \mu_2^2(1+\nu b)} c_1 - \frac{1}{\nu b} \exp\left[-\frac{1}{2}t\right] c_2 \tag{76}$$

$$+ \left(\frac{a_2 - 2a_1 a_2 \mu_1}{-2\mu_2^2 + a_2 \nu b}\right) \exp\left[t\left(-\frac{1}{2} - a_1\mu_1 - \frac{\mu_2^2}{a_2}\right)\right] c_3 - \exp\left[t\left(-1 - \frac{\nu b}{2}\right)\right] c_5$$

$$p_2 = \frac{2a_1 a_2 \mu_1 + \mu_2^2}{a_1 a_2 \mu_1 \nu b + \mu_2^2(1+\nu b)} c_1 + \frac{1}{\nu b} \exp\left[-\frac{1}{2}t\right] c_2 \tag{77}$$

$$+ \left(\frac{a_2 - 2a_1 a_2 \mu_1}{-2\mu_2^2 + a_2 \nu b}\right) \exp\left[t\left(-\frac{1}{2} - a_1\mu_1 - \frac{\mu_2^2}{a_2}\right)\right] c_3 - \exp\left[t\left(-1 - \frac{\nu b}{2}\right)\right] c_4$$

$$p_3 = c_1 - \exp\left[-\frac{1}{2}t\right] c_2 + \exp\left[t\left(-\frac{1}{2} - a_1\mu_1 - \frac{\mu_2^2}{a_2}\right)\right] c_3 + \exp\left[t\left(-1 - \frac{\nu b}{2}\right)\right] c_5 \tag{78}$$

$$p_3 = c_1 + \exp\left[-\frac{1}{2}t\right] c_2 + \exp\left[t\left(-\frac{1}{2} - a_1\mu_1 - \frac{\mu_2^2}{a_2}\right)\right] c_3 + \exp\left[t\left(-1 - \frac{\nu b}{2}\right)\right] c_4 \tag{79}$$

where

$$c_1 = -\frac{-\mu_2^2 - a_1 a_2 \mu_1 \nu b - \mu_2^2 \nu b}{\left(a_2 + 2a_1 a_2 \mu_1 + 2\mu_2^2\right)(2+\nu b)} \tag{80}$$

$$c_2 = -\frac{\nu b}{2(1+\nu b)} \tag{81}$$

$$c_3 = -\frac{a_2\left(-2\mu_2^2 + a_2 \nu b\right)}{2\left(a_2 + 2a_1 a_2 \mu_1 + 2\mu_2^2\right)\left(-a_2 + 2a_1 a_2 \mu_1 + 2\mu_2^2 - a_2 \nu b\right)} \tag{82}$$

$$c_4 = -\frac{-\mu_2^2 + a_1 a_2 \mu_1 \nu b}{(1+\nu b)(2+\nu b)\left(a_2 - 2a_1 a_2 \mu_1 - 2\mu_2^2 + a_2 \nu b\right)} \tag{83}$$

$$c_5 = \frac{\mu_2^2 - 2a_2 \nu b + 3a_1 a_2 \mu_1 \nu b + 4\mu_2^2 \nu b - 3a_2 \nu^2 b^2 + 2a_1 a_2 \mu_2^2 \nu b^2 + 2\mu^2 \nu b^2 - a_2 \nu^3 b^3}{(1+\nu b)(2+\nu b)\left(a_2 - 2a_1 a_2 \mu_1 - 2\mu_2^2 + a_2 \nu b\right)} \tag{84}$$

Appendix II

The Boltzmann-Gibbs entropy relation, which holds for systems far from equilibrium, is expressed as

$$S[p_i(t)] = -\sum_{i=1}^{3} p_i \ln p_i \tag{85}$$

Differentiating Equation (1) with respect to time yields

$$\dot{S}(t) = \dot{e}_p(t) - \dot{h}(t) = \sum_{i>j} (p_i P_{ji} - p_j P_{ij}) \ln\left(\frac{p_i}{p_j}\right) \tag{86}$$

where $\dot{S}(t)$ represents the rate of change in entropy. The entropy extraction rate $\dot{h}_d(t)$ is given by

$$\dot{h}_d(t) = -\frac{\dot{Q}_h(t)}{T_h} + \frac{\dot{Q}_c(t)}{T_c} = \sum_{i>j} (p_i P_{ji} - p_j P_{ij}) \ln\left(\frac{P_{ji}}{P_{ij}}\right) \tag{87}$$

where $\dot{Q}_h(t)$ and $\dot{Q}_c(t)$ denote the heat absorbed from the hot reservoir and heat transferred to the cold reservoir, respectively. The entropy production rate $\dot{e}_p(t)$ is given by

$$\dot{e}_p(t) = \sum_{i>j} (p_i P_{ji} - p_j P_{ij}) \ln\left(\frac{p_i P_{ji}}{p_j P_{ij}}\right). \tag{88}$$

We want to stress that the entropy, entropy production rate, and entropy extraction rate are defined using the full probability distribution and transition rates between states. These quantities are expressed as explicit functions of time, temperature gradient, external load, and the system's microscopic dynamics. The model generally considers time-dependent behavior; however, in the limit where $t \to \infty$, and when $T_h \neq T_c$ or a non-zero external force is applied, the system reaches a nonequilibrium steady state. In that regime, the entropy-related quantities approach constant values, and the definitions naturally reduce to their steady-state forms.

When the expressions for the probability distributions and transition rates for networks of different sizes are substituted into the formulas for entropy production rate, entropy extraction rate, and velocity, we find that all these thermodynamic rates are independent of the system size M.

The results of this study indicate that the rates of entropy change $\dot{S}(t)$, heat dissipation $\dot{h}_d(t)$, and entropy production $\dot{e}_p(t)$ are the highest for an exponentially decreasing temperature case. At steady state, irrespective of the temperature profile, both the entropy production and heat dissipation rates remain positive: $\dot{e}_p(t) = \dot{h}_d(t) > 0$. In the absence of a load and under isothermal conditions, both rates reduce to zero at the steady state: $\dot{e}_p(t) = \dot{h}_d(t) = 0$.

By integrating the above rates with respect to time, we get the corresponding extensive thermodynamic relations

$$\Delta h_d(t) = \int_{t_0}^{t} \dot{h}_d(t)dt \tag{89}$$

$$\Delta e_p(t) = \int_{t_0}^{t} \dot{e}_p(t)dt \tag{90}$$

$$\Delta S(t) = \int_{t_0}^{t} \dot{S}(t)dt \tag{91}$$

where $\Delta S(t) = \Delta e_p(t) - \Delta h_d(t)$.

These thermodynamic quantities depend on the network size.

The term that is related to the heat dissipation rate can be expressed as

$$\dot{H}_d(t) = \sum_{i>j} T_j(p_i P_{ji} - p_j P_{ij}) \ln\left(\frac{P_{ji}}{P_{ij}}\right) = \dot{E}_p(t) - \dot{S}^T(t) \tag{92}$$

where

$$\dot{E}_p(t) = \sum_{i>j} T_j(p_i P_{ji} - p_j P_{ij}) \ln\left(\frac{p_i P_{ji}}{p_j P_{ij}}\right) \tag{93}$$

$$\dot{S}^T(t) = \sum_{i>j} T_j(p_i P_{ji} - p_j P_{ij}) \ln\left(\frac{p_i}{p_j}\right) \tag{94}$$

Integrating the above rates with respect to time, leads to

$$\Delta H_d(t) = \int_{t_0}^{t} \dot{H}_d(t)dt, \tag{95}$$

$$\Delta E_p(t) = \int_{t_0}^{t} \dot{E}_p(t)dt, \tag{96}$$

$$\Delta S^T(t) = \int_{t_0}^{t} \dot{S}^T(t)dt. \tag{97}$$

The total internal energy $U(t)$ is given by

$$U[p_i(t)] = \sum_{i=1}^{3} p_i u_i, \tag{98}$$

with the change in the internal energy

$$\Delta U(t) = U[p_i(t)] - U[p_i(0)]. \tag{99}$$

The first law of thermodynamics is verified as

$$\dot{U}[P_i(t)] = -\sum_{i>j}(p_i P_{ji} - p_j P_{ij})(u_i - u_j) = -(\dot{H}_d(t) + fV(t)). \tag{100}$$

For free energy dissipation, adapting the isothermal case $F = U - TS$ to the non-isothermal case gives

$$\dot{F}(t) = \dot{U}(t) - \dot{S}^T(t). \tag{101}$$

After simplifications:

$$\dot{F}(t) + \dot{E}_p(t) = \dot{U}(t) + \dot{H}_d(t) = -fV(t). \tag{102}$$

The change in free energy is

$$\Delta F(t) = \int_{t_0}^{t} \left(-fV(t) - \dot{E}_p(t)\right) dt = \Delta U + \Delta H_d - \Delta E_p. \tag{103}$$